A ~580 kyr paleomagnetic record from the sub-Antarctic South Atlantic (Ocean Drilling Program Site 1089)

J. S. Stoner[1]
Department of Geology, University of California, Davis, California, USA

J. E. T. Channell and D. A. Hodell
Department of Geological Sciences, University of Florida, Gainesville, Florida, USA

C. D. Charles
Scripps Institution of Oceanography, La Jolla, California, USA

Received 27 September 2001; revised 4 April 2002; accepted 13 November 2002; published 14 May 2003.

[1] We report geomagnetic directional paleosecular variation, relative paleointensity proxies and oxygen isotope data from the upper 88 m composite depth (mcd) at South Atlantic Ocean Drilling Program (ODP) Site 1089 (40°56.2′S, 9°53.64′E, 4620 m water depth). The age model is provided by high-resolution oxygen isotope stratigraphy, augmented by radiocarbon dates from the upper 8 mcd of nearby piston core RC11-83. Mean sedimentation rates at Site 1089 are in the range of 15 to 20 cm/kyr. Two intervals during the Brunhes Chron, at ~29.6 mcd (~190 ka) and at ~48 mcd (~335 ka), have component magnetization directions with positive (reverse polarity) inclination; however, the excursional directions are heavily overprinted by the postexcursional field. Magnetite is the dominant carrier of magnetic remanence, and occurs in the pseudosingle-domain (PSD) grain size. An additional higher-coercivity magnetic carrier, characterized by low unblocking temperatures (<350°C), is assumed to be authigenic pyrrhotite. A decrease in magnetization intensity down core is mirrored by a reduction in pore water sulfate, indicating diagenetic reduction of magnetite. Despite down-core changes in magnetic mineralogy, normalized intensity records from Site 1089 are comparable with high-resolution paleointensity records from the North Atlantic (e.g., ODP Sites 983 and 984). Sediment properties and sedimentation patterns within the Cape (Site 1089) and Iceland (Sites 983 and 984) Basins are distinctly different at both millennial and orbital timescales and therefore preclude lithologic variability from being the source of this correlation. Variations in normalized intensity from Site 1089 therefore appear to reflect changes in global-scale geomagnetic field intensity. *INDEX TERMS:* 1512 Geomagnetism and Paleomagnetism: Environmental magnetism; 1513 Geomagnetism and Paleomagnetism: Geomagnetic excursions; 1520 Geomagnetism and Paleomagnetism: Magnetostratigraphy; 1521 Geomagnetism and Paleomagnetism: Paleointensity; 1522 Geomagnetism and Paleomagnetism: Paleomagnetic secular variation; *KEYWORDS:* geomagnetic paleointensity, paleomagnetic secular variation, paleomagnetic excursions, Pleistocene, South Atlantic Ocean, oxygen isotope stratigraphy

Citation: Stoner, J. S., J. E. T. Channell, D. A. Hodell, and C. D. Charles, A ~580 kyr paleomagnetic record from the sub-Antarctic South Atlantic (Ocean Drilling Program Site 1089), *J. Geophys. Res.*, *108*(B5), 2244, doi:10.1029/2001JB001390, 2003.

1. Introduction

[2] Relative paleointensity records appear to reflect changes in the global-scale geomagnetic field and these changes can be used to synchronize paleoclimate records at millennial timescales [e.g., *Channell et al.*, 2000; *Laj et al.*, 2000; *Stoner et al.*, 2000]. Geomagnetic excursions, if demonstrated to be manifest globally, could provide "golden spikes" for stratigraphic correlation. Directional secular variation may provide synchronization to the centennial level, but over limited geographic areas [e.g., *Lund*, 1996]. At present, secular variation is mostly used for correlation during the Holocene. Of the geomagnetic excursions, only the Laschamp event at ~40 ka has been observed over a wide enough area with tight enough stratigraphic control to be considered a global stratigraphic marker [e.g., *Channell et al.*, 2000; *Laj et al.*, 2000]. Long-period (>10 kyr) variations in relative paleointensity have been shown to be globally correlative for the last

[1]Now at Institute of Arctic and Alpine Research (INSTAAR), University of Colorado, Boulder, Colorado, USA.

0148-0227/03/2001JB001390$09.00

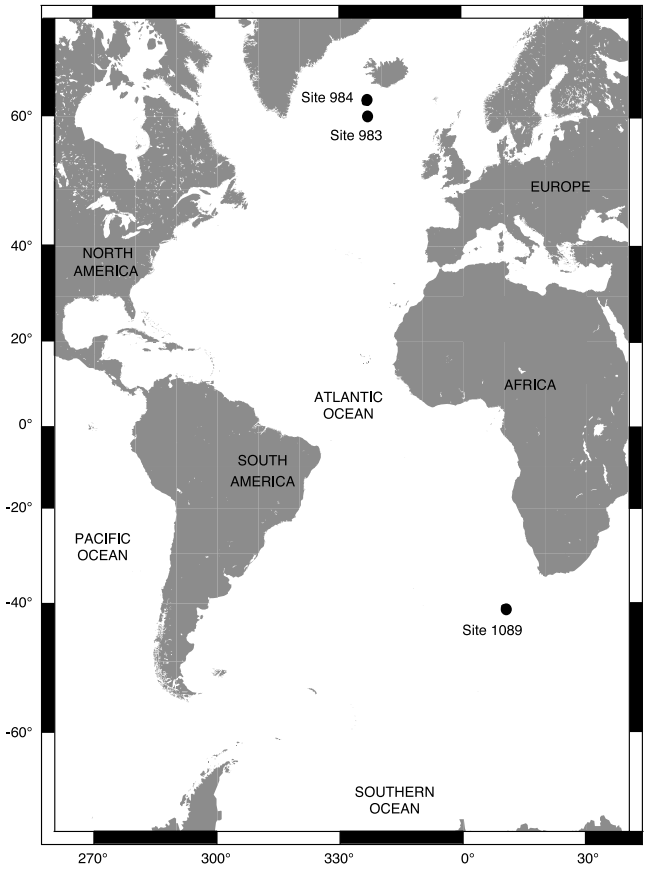

Figure 1. Location of ODP Sites 1089, 983, and 984.

800 kyr [*Guyodo and Valet*, 1999] but a case for global correlation at millennial scale can only be made for last the 100 kyr [*Stoner et al.*, 2000].

[3] High sedimentation rate piston cores from the sub-Antarctic South Atlantic, acquired during the site survey cruise for Ocean Drilling Program (ODP) Leg 177, have provided records of relative geomagnetic paleointensity and directional secular variation from the midlatitude Southern Hemisphere for the last 100 kyr [*Channell et al.*, 2000]. These records demonstrate global-scale changes in relative geomagnetic paleointensity at timescales of 10^3 years, and can be used in concert with other stratigraphic methods to improve stratigraphic resolution [*Channell et al.*, 2000; *Stoner et al.*, 2000]. These conventional piston core records do not extend beyond 100 ka because of high sedimentation rates (15–25 cm/kyr). However, the advanced piston corer (APC) utilized by ODP can recover undisturbed sediment from much greater depths. Here we report a u-channel-based paleomagnetic study, from Site 1089 (ODP Leg 177) that extends the paleointensity record from the sub-Antarctic South Atlantic to ~580 ka.

[4] Site 1089 (latitude 40°56.2′S, longitude 9°53.6′E, water depth 4624 m) is located in the southern Cape Basin on the northern flank of the Agulhas Ridge (Figure 1). The site is situated in the northern sub-Antarctic Zone between the Subtropical Front (STF) to the north and the sub-Antarctic Front (SF) to the south. Because of the high mean sediment accumulation rates (~15 cm/kyr) and good carbonate preservation, this site provides a high-resolution climate record for the Southern Hemisphere analogous to those from North Atlantic sites drilled during ODP Legs 162 and 172. During the last glacial interval, planktic ($\delta^{18}O$) and benthic ($\delta^{13}C$) isotope data from piston core (RC11-83), located close to Site 1089, record millennial-scale climate variations that were interpreted as characteristic of both the southern (sea surface temperature changes) and northern (variations in the flux of North Atlantic Deep Water) hemispheres, respectively [*Charles et al.*, 1996]. On the basis of this study, it was suggested that the warm part of millennial-scale climate oscillations in the sub-Antarctic South Atlantic leads similar warming observed in the North Atlantic and Greenland ice cores by 1500 years during Marine Isotopic Stage (MIS) 3. One of the main objectives at Site 1089 was to extend this pioneering study back in time, to look at the millennial-scale climate system, as recorded at this unique site, through a full range of background (glacial, interglacial, transitional) climate states [e.g., *Ninnemann et al.*, 1999; *Mortyn et al.*, 2003]. If this is to be fully accomplished, it will be necessary to derive independent millennial-scale stratigraphic control beyond the limit of radiocarbon dating.

[5] Here we present oxygen isotope data and paleomagnetic and rock magnetic data from Site 1089. The magnetic record is affected by magnetite dissolution and secondary growth of authigenic iron sulfides; however, two intervals of excursional magnetic directions are recorded and normalized remanence records are consistent using different normalizers and normalization methods. Correlation of the normalized remanence record from Site 1089 to relative paleointensity records from the Northern Hemisphere indicate that global-scale changes in geomagnetic field strength are recorded.

2. Lithology and Age Models

[6] Site 1089 is located on a gently sloping sediment drift on the southeastern flank of the Agulhas Ridge (Figure 1). The sediment comprises pale to very pale gray, greenish tan and olive green nannofossil ooze with varying amounts of mud and siliceous components. Alternating dark and light beds represent variations in biogenic to terrigenous input ratio on glacial-interglacial timescales [*Shipboard Scientific Party*, 1999]. The top 40 cm has a light yellowish-brown color associated with core top oxidizing conditions. Carbonate varies from near 0% to 70%, averaging around 20%, and is essentially the inverse of the magnetic susceptibility signal suggesting a relatively constant terrigenous supply [*Hodell et al.*, 2001] (Figure 2). Mud content varies from 2% to 80% and nannofossil content from 0% to 90%. Evidence for bioturbation is prevalent and pyrite molds and pyrite are relatively common [*Shipboard Scientific Party*, 1999].

[7] Planktic oxygen isotope measurements were carried out on monospecific samples of *Globigerina bulloides* selected from the 212–300 μm size fraction. Benthic oxygen isotope measurements were made on benthic foraminifera, using specimens of *Cibicidoides wuellerstorfi* and *C. kullenbergi* selected from the >150 μm size fraction. The upper 37.5 m (mcd) were analyzed at Scripps Institute

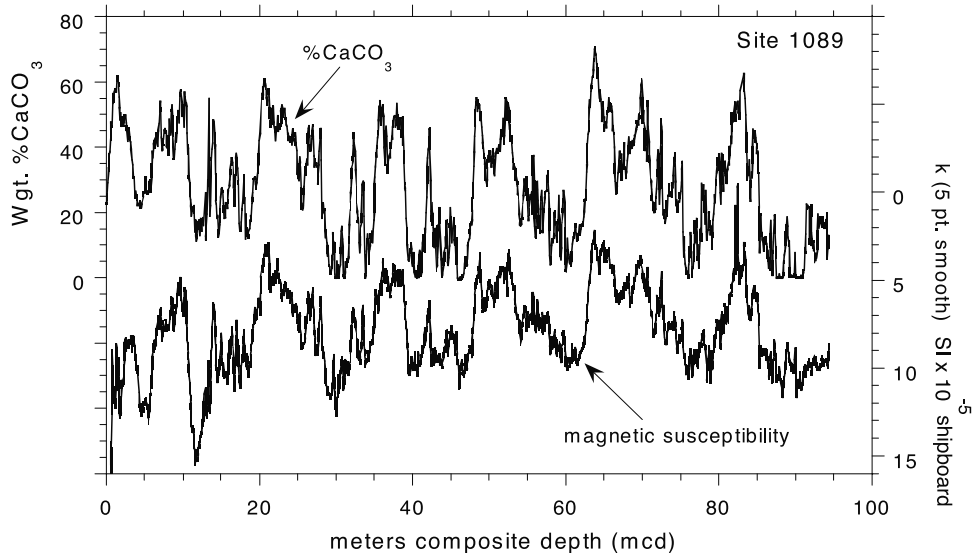

Figure 2. Weight percent $CaCO_3$ compared with shipboard derived whole core magnetic susceptibility.

of Oceanography, whereas the sediments below that level were measured at the University of Florida. Methods of stable isotopic analysis are described by *Hodell et al.* [2003] and *Mortyn et al.* [2003].

[8] The age model for Site 1089 is based on correlating the benthic and planktic oxygen isotope records to the SPECMAP reference curve [*Imbrie et al.*, 1984; *Martinson et al.*, 1987]. Continuous correlation to SPECMAP for the last 190 kyr results in a well-constrained age model during this time interval (Figure 3). For the upper 11 mcd, this was augmented by correlating the planktic and benthic oxygen isotope data from Site 1089 to those from nearby cores RC11-83 (41°36′S, 9°48′E) [*Charles et al.*, 1996] and TNN057-21-PC02 (21-PC02) (41°8′S, 7°48′E) [*Channell et al.*, 2000; *Mortyn et al.*, 2003]. RC11-83 has 14 radiocarbon ages in the 11–41 ka interval and an identifiable 4/3 marine isotopic stage (MIS) boundary. Core 21-PC02 provides a benthic record and an identifiable 5/4 MIS boundary [*Ninnemann et al.*, 1999]. Intense carbonate dissolution and scarcity of benthic foraminifera during MIS 7 prevented the development of a continuous benthic oxygen isotope record. The age model for MIS 7, between ~190 and 220 kyr, is based on correlation of the planktic $\delta^{18}O$ signal to the reference curve (Figure 3). Below 30 mcd (~190 ka) correlation to SPECMAP is based on 15 tie points and linear sedimentation rate between tie points (Figure 3) [*Hodell et al.*, 2001]. On the basis of these correlations, interval sedimentation rates range from 5 to >30 cm/kyr (Figure 3).

3. Magnetic Measurements

[9] The archive halves of core sections from the composite section at Site 1089 were sampled using plastic u channels [*Tauxe et al.*, 1983]. Magnetic measurements were carried out at 1 cm intervals on an automated 2G Enterprises "u channel" cryogenic magnetometer at the University of California, Davis. During routine shipboard measurements, the archive halves were demagnetized with peak alternating fields (AF) of 20 mT [*Shipboard Scientific Party*, 1999]. The natural remanent magnetization (NRM) of u channel samples was measured to monitor the (viscous) magnetization acquired during storage. Alternating field (AF) demagnetization was begun at peak fields of 20 mT, progressing stepwise at 2.5 mT increments to 40 mT, then 5 mT increments to 50 mT, and either 5 or 10 mT increments to either 80 mT or 100 mT. Anhysteretic remanent magnetization (ARM) was then imposed using a 100 mT peak AF and a 0.05 mT direct current (DC) biasing field. The ARM was measured, then remeasured after AF demagnetization at peak fields of 10, 20, 25, 30, 35, 40, 50, 60, 70, and 80 mT. The ARM data are also presented as an anhysteretic susceptibility (k_{ARM}) by normalizing by the DC biasing field. Isothermal remanent magnetization (IRM) was produced in a pulsed DC field of 0.3 T ($IRM_{0.3T}$) and 1T (IRM_{1T}) (for the upper 21 mcd). The IRMs were measured, then remeasured after AF demagnetized at peak fields of 10, 20, 25, 30, 35, 40, 50, 60, 70, and 80 mT. To compare shipboard whole core magnetic susceptibility with u channel data, the magnetic susceptibility measurements, were linearly interpolated to 1 cm intervals of the u channel measurements and multiplied by an empirically determined factor 6.8×10^{-6} to convert data into SI volume units (k). To better characterize the magnetic mineralogy, discrete samples from the lower part of the section were thermally demagnetized after AF demagnetization. Hysteresis measurements and IRM acquisition curves were produced using a Princeton Measurements Corporation Alternating Gradient Magnetometer ("MicroMag").

4. Magnetic Properties

[10] Orthogonal projection of stepwise alternating field (AF) demagnetization of discrete samples taken from the working halves of core sections from Site 1089 indicate that a steep downward magnetic overprint was removed

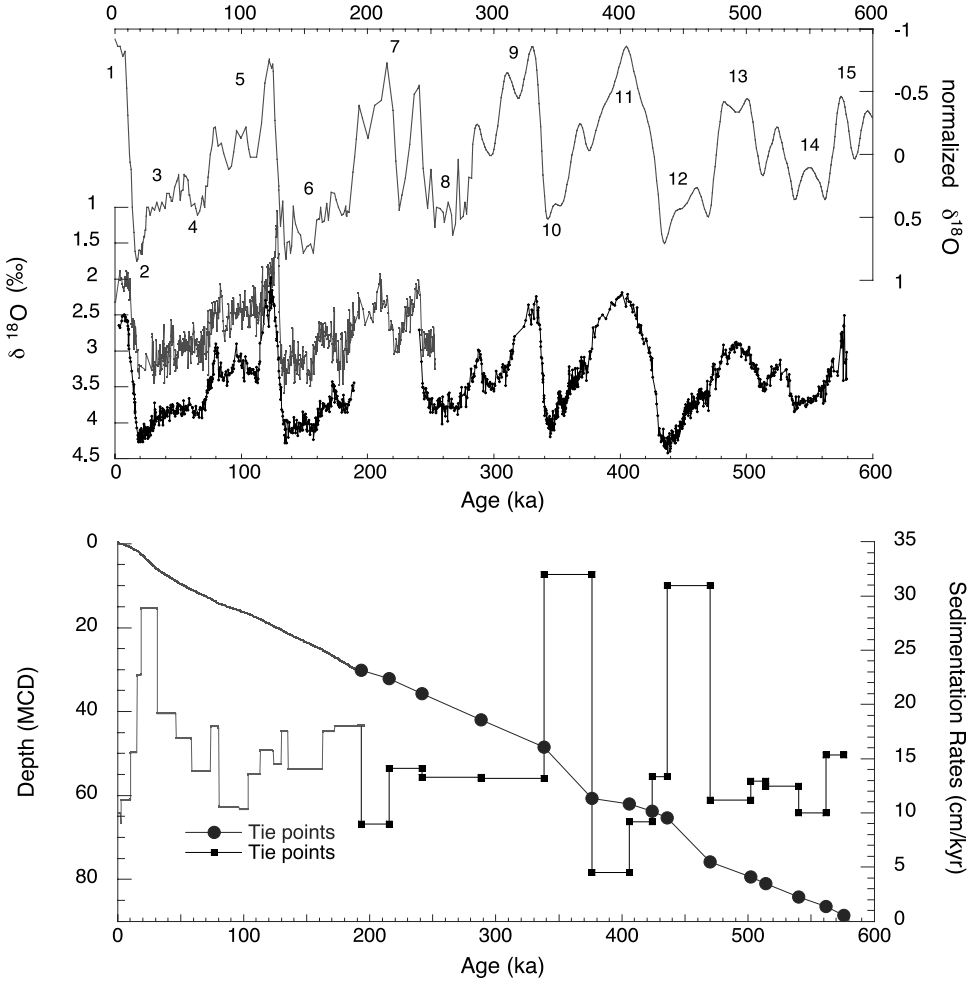

Figure 3. (top) Planktic $\delta^{18}O$ from *Globigerina bulloides* and benthic $\delta^{18}O$ *Cibicidoides wuellerstorfi* and *C. kullenbergi* for Site 1089 [see *Hodell et al.*, 2001; *Mortyn et al.*, 2003]. Ages are based on correlation of $\delta^{18}O$ at 1089 to the SPECMAP reference isotope curve (top) [*Imbrie et al.*, 1984; *Martinson et al.*, 1987]. Numbers indicate corresponding marine isotopic stage. (bottom) Age depth relationship and interval sedimentation rate based on the age model. See color version of this figure in the HTML.

at low peak fields (5–10 mT) (Figure 4b). This drilling induced magnetic overprint is not observed in the u channel samples (Figure 4a) and was therefore removed during routine shipboard demagnetization of the archive halves prior to u channel sampling. Prior to shipboard demagnetization, NRM intensities were in the 10^{-3} to 10^{-4} A/m range for all but the upper 2 mcd, where NRM intensities were $\sim 10^{-2}$ A/m [*Shipboard Scientific Party*, 1999; *Channell and Stoner*, 2002]. Initial intensities of the u channel samples (after shipboard AF demagnetization at peak fields of 20 mT) are also in the 10^{-3} to 10^{-4} A/m range (Figures 4 and 5). Data from the shipboard pass-through magnetometer, and discrete samples measurements, have led to a straightforward interpretation of magnetic polarity stratigraphy to the base of the Olduvai Subchron [*Channell and Stoner*, 2002].

[11] Orthogonal projections of NRM demagnetization data indicate the presence of both low- and high-coercivity magnetization components, with an increase in proportion of the high-coercivity component down core (Figure 4a). Thermal demagnetization, after AF demagnetization on discrete samples toward the base of the section, demonstrates that the high-coercivity component has blocking temperatures below 350°C, consistent with an iron sulfide, presumably pyrrhotite (Figure 4b). Isothermal remanent magnetization (IRM) acquisition curves (Figure 6) indicate that a high-coercivity remanence carrier does not saturate by 300 mT. A sample from 1.26 mcd displays lower coercivities than other samples measured in the 6.82–62.72 mcd depth range. Hysteresis ratios lie in the pseudosingle-domain (PSD) field of the *Day et al.* [1977] plot (Figure 7); however, the distribution is scattered and does not lie along the usual single-domain (SD) to multidomain (MD) mixing line. The shallower slope of the trend, relative to that expected for a SD/MD mixing line, is consistent with the influence of a higher-coercivity (pyrrhotite) and PSD magnetite magnetic mineralogy [*Channell and McCabe*, 1994].

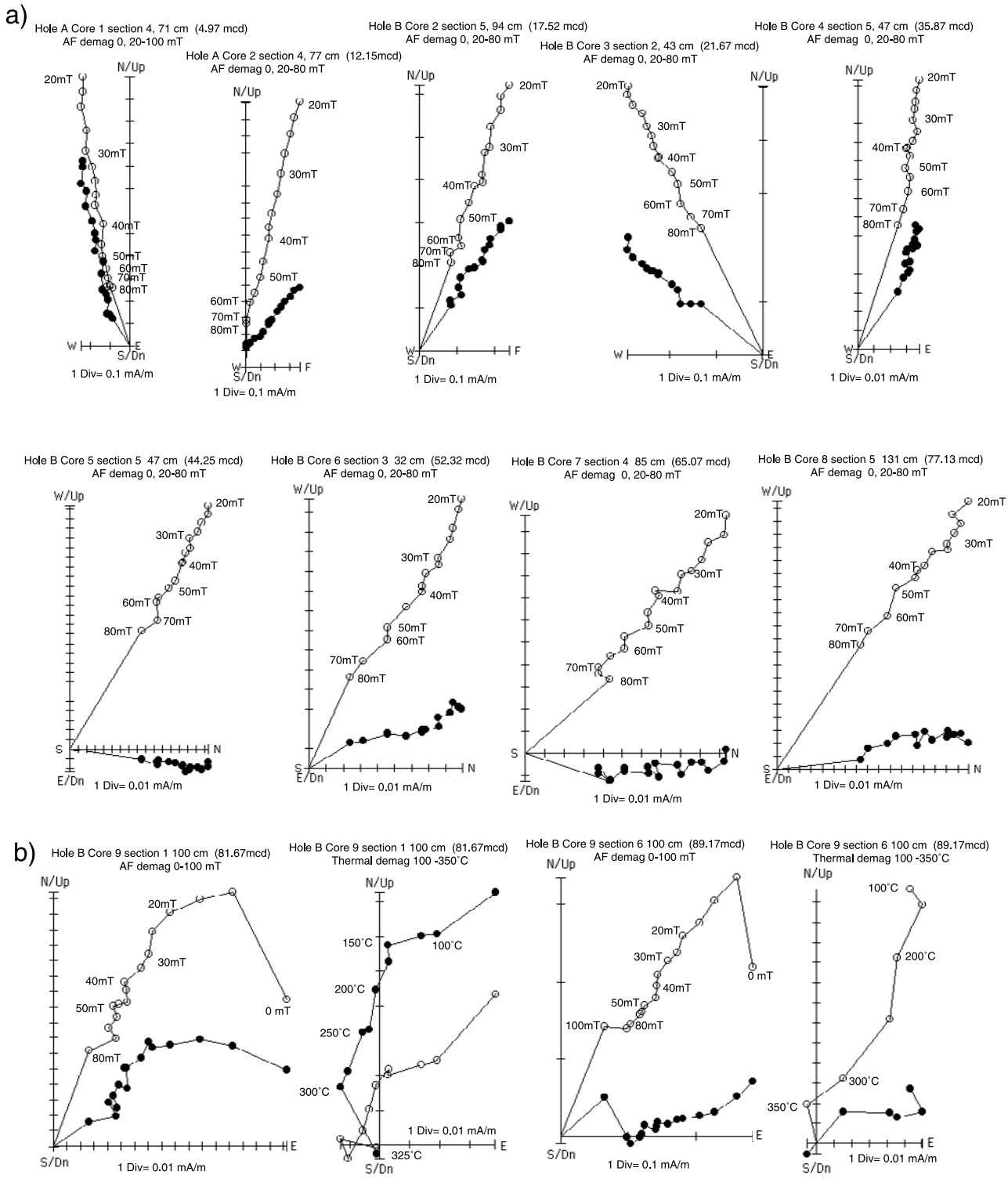

Figure 4. (a) Orthogonal projection of selected alternating field demagnetization data from u channel measurements for the composite section at Site 1089. Open and solid symbols indicate projection of vector endpoints on the vertical and horizontal planes, respectively. Declinations have been corrected for a core mean of 0 as described in text. The magnetization intensity associated with one division on the axes of each plot is indicated. (b) Orthogonal projection of demagnetization data for discrete samples from Hole 1089B. Samples were first demagnetized using (left) alternating fields and (right) the remaining remanence was then thermally demagnetized. Open and solid symbols indicate projection of vector endpoints on the vertical and horizontal planes, respectively. Declinations have not been corrected. Peak alternating fields are indicted in mT and temperatures in °C.

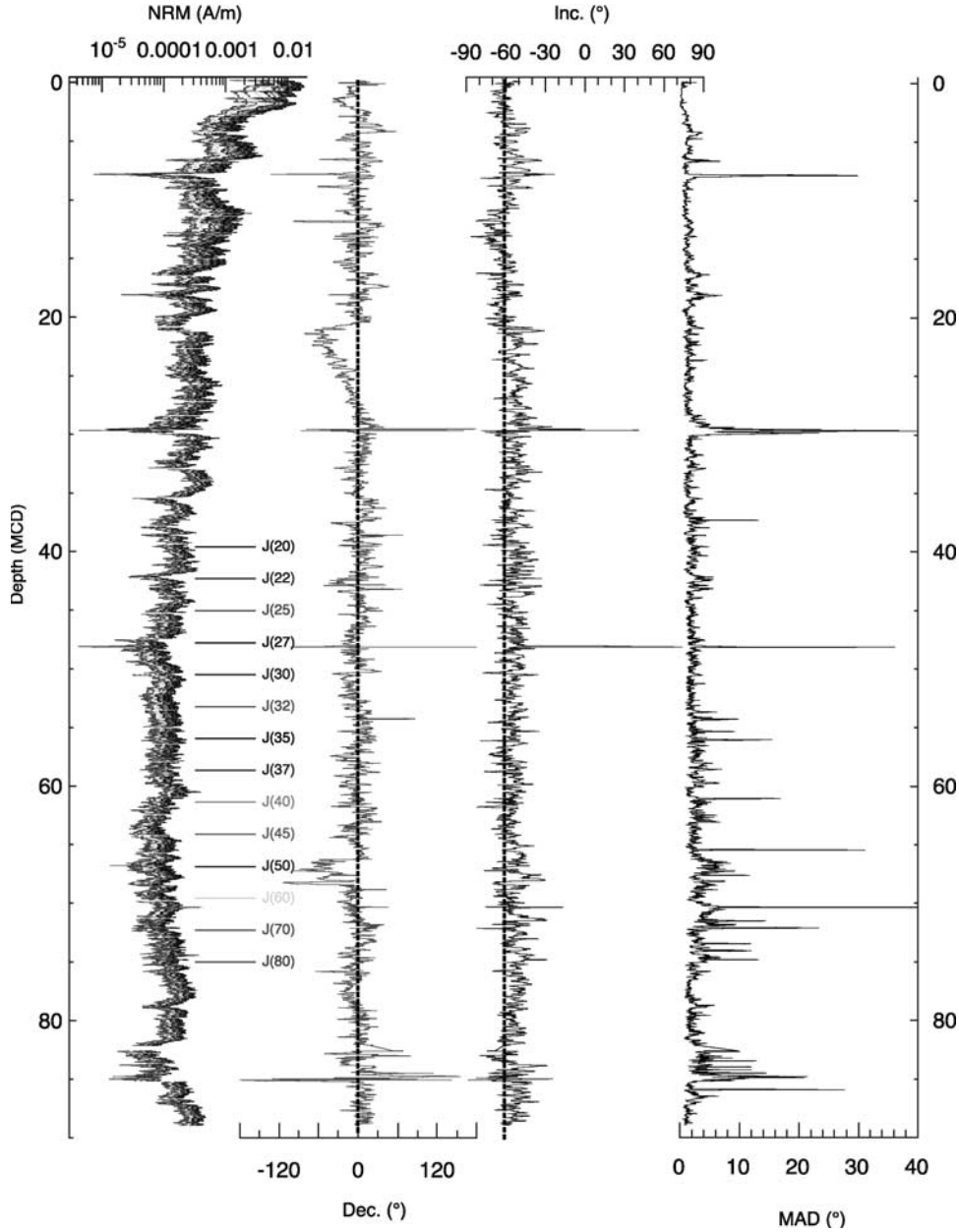

Figure 5. Site 1089. NRM intensities after stepwise alternating field demagnetization in (left) the 20–80 mT interval and (middle) component declination and inclination and (right) the associated maximum angular deviation (MAD) values calculated for AF demagnetization at peak demagnetization fields in the 25–50 mT interval. Vertical line indicates expected inclination (60°) for site latitude. See color version of this figure in the HTML.

[12] Concentration-dependent magnetic parameters (ARM and IRM) indicate that there is a significant decrease in remanence intensity with depth (Figure 8). Much of the decrease occurs over 3 steps (step 1 at ~0.77 mcd, step 2 at ~1.35 mcd, step 3 at ~2.5 mcd). The third step results in the largest remanence drop and is more gradational than the other two, occurring from ~1.9 to 2.9 mcd. This last step results in a intensity drop of ~90% for the NRM (from 0.011 to 0.001 A/m) and ARM (from 0.11 to 0.01 A/m), 55% for the $IRM_{0.3T}$ (from 1.6 to 0.7 A/m), and 30% for k (12 to 8.5 $\times$ 10^{-5} SI) (Figures 5 and 8). Below this level, there is a gradual loss in remanence intensity down to ~40 mcd. Below 40 mcd, remanence intensities reach steady state, varying around an essentially constant mean value. Superimposed on the long-term trend are glacial-interglacial changes in concentration, particularly apparent in the susceptibility record (Figures 2 and 8). These changes in magnetic concentration are consistent with dilution due to variable biogenic carbonate content [*Hodell et al.*, 2001; *Kuhn and Diekman*, 2002]. The magnetic grain-size sensitive ratio k_{ARM}/k (Figure 8) also displays an abrupt decrease at

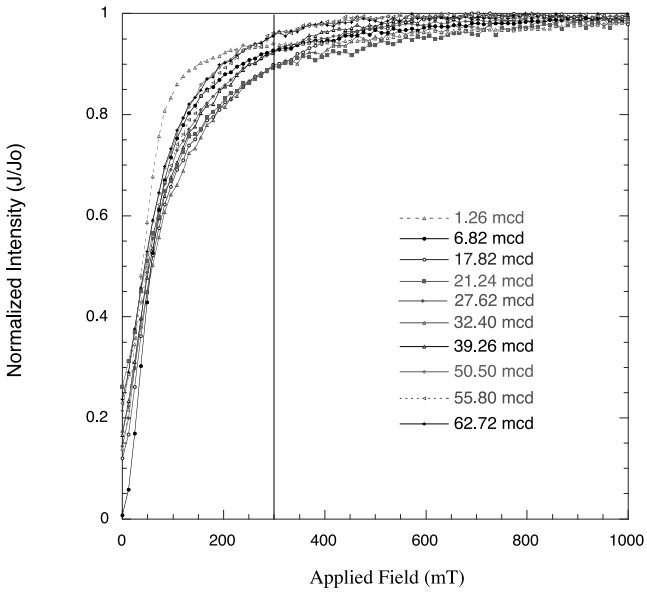

Figure 6. Normalized isothermal remanent magnetization (IRM) acquisition curves of selected samples from Site 1089. Vertical line at 300 mT is for reference. See color version of this figure in the HTML.

~2.5 mcd, followed by a gradual down-core decrease to ~40 mcd, suggesting a coarsening of magnetite grain size, due to dissolution of fine grained magnetite. The susceptibility record is less affected by the dissolution process as it is dominated by the coarser magnetite grain-size fraction.

[13] Magnetic properties and magnetic concentration change significantly in the uppermost part of the section, down to 2.8 mcd. This difference is well illustrated on a plot of anhysteretic susceptibility (k_{ARM}) versus volume susceptibility (k) [*Banerjee et al.*, 1981; *King et al.*, 1983]. In Figure 9, we have drawn lines indicating the values of k_{ARM}/k corresponding to ~2 μm and ~15–20 μm magnetite grain sizes, based on the estimates of *King et al.* [1983]. Because of the presence of iron sulfides these estimates should be taken with caution, nonetheless, the data suggest a much finer magnetite assemblage above 2.8 mcd, with progressive coarsening of the magnetite assemblage down core. Below ~7 mcd, the magnetite assemblage appears to lie in the 2–20 μm grain-size range (Figure 9). The coarsening of magnetite grain size is attributed to the preferential dissolution of fine grains, due to the greater surface area to volume ratio. Pore water sulfate concentrations at Site 1089 fall from seawater values (~24 mM) at the sediment-water interface to values close to zero between 40 and 50 mcd [*Shipboard Scientific Party*, 1999]. The reduction of pore water sulfate to sulfide is mirrored by a reduction of magnetization intensity and an increase in magnetite grain size (Figures 5, 8, and 9). We infer that microbial sulfate reduction (to sulfide) results in dissolution of fine-grained magnetite and formation of authigenic iron sulfides. The ultrafine-grained magnetite in the surface sediment may be biogenic in origin, with this component being essentially restricted to the uppermost 2.8 m of the sediment sequence.

5. Natural Remanent Magnetization (NRM) Directions

[14] Orthogonal projection of stepwise alternating field (AF) demagnetization from u channel data indicate that the characteristic magnetization component is well defined (Figure 4). NRM component directions (Figure 4) were calculated at 1 cm intervals for nine demagnetization steps between 25 and 50 mT using the standard least squares method [*Kirschvink*, 1980]. Maximum angular deviation (MAD) values are below 10° for all but a few discrete intervals, and generally below 5°. For the upper 21 mcd,

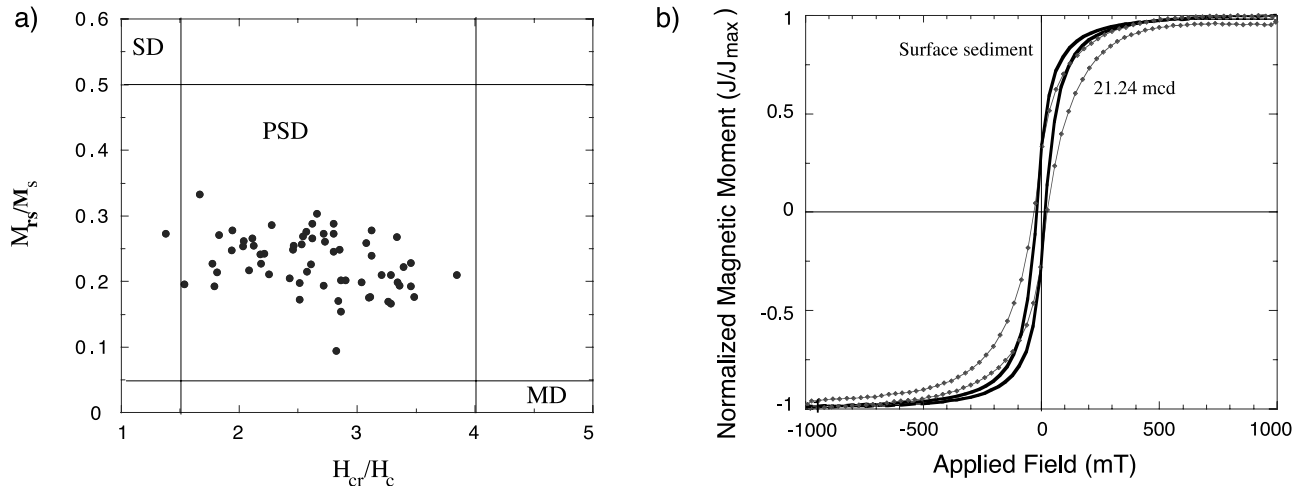

Figure 7. (a) Hysteresis ratios based on remanent magnetization (M_{rs}), saturation magnetization (M_s), coercivity of remanence (H_{cr}), and coercivity (H_c) for Sites 1089, plotted relative to the single-domain (SD), pseudosingle-domain (PSD), and multidomain (MD) fields for magnetite [after *Day et al.*, 1977]. (b) Normalized hysteresis loops from a surface sediment sample (at Site 1089) and a sample at 21.24 mcd. See color version of this figure in the HTML.

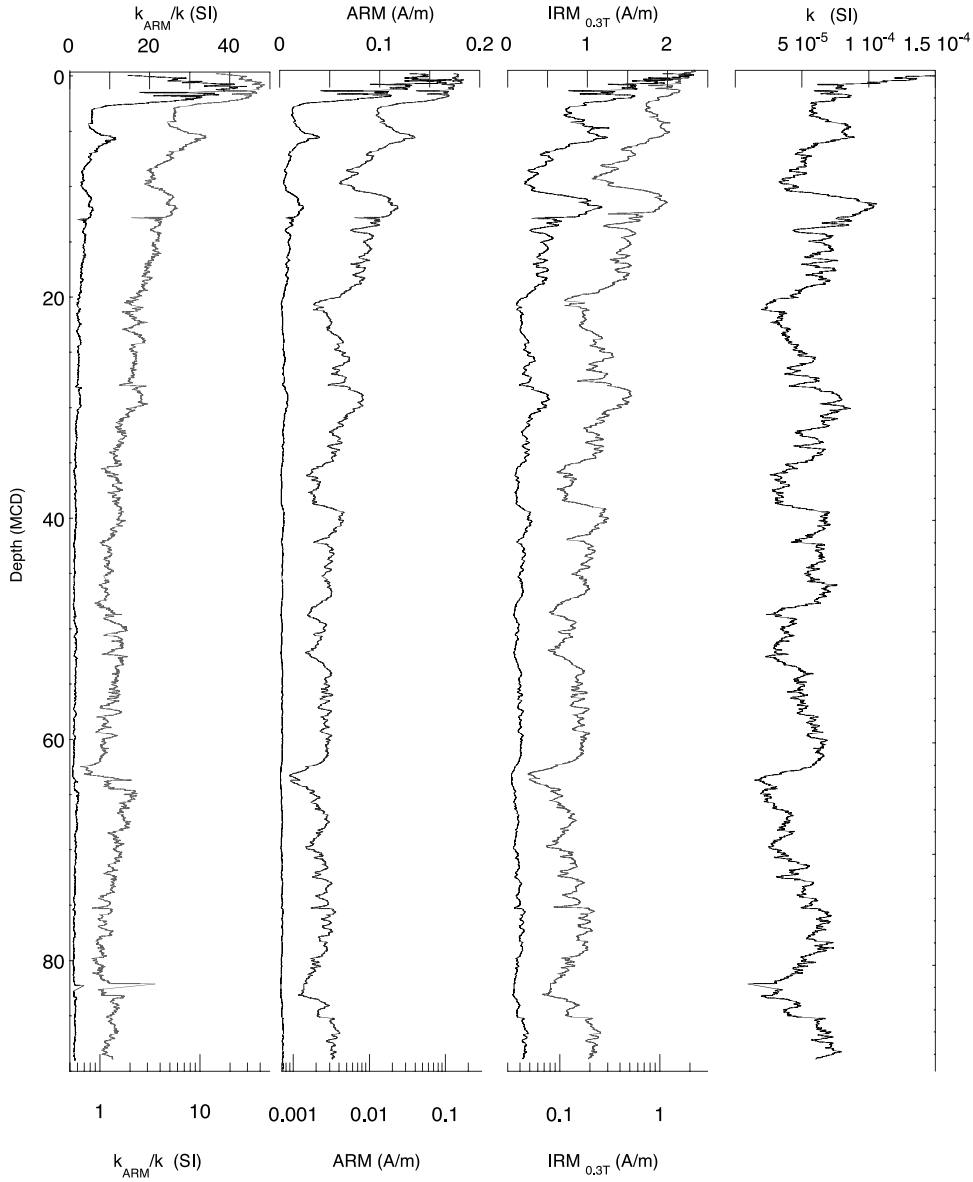

Figure 8. Site 1089. ARM and IRM intensities and the ratio of anhysteretic susceptibility to magnetic susceptibility (k_{ARM}/k) on linear (left curves) and log (right curves) scales and shipboard whole core magnetic susceptibility (k) plotted against depth (mcd). See color version of this figure in the HTML.

the inclination values vary about the expected geocentric axial dipole mean inclination (60°) for the site latitude (Figure 5). Below 20.5 mcd, inclination values are, on average, ~6°shallower than expected.

[15] Declinations were corrected to account for core to core rotation by matching, where possible, overlapping sections within the sampled splice. Because of sporadic shipboard orientation data, absolute azimuth orientations were only available for three of the cores used within the splice. For two of these cores, the orientation data are consistent with average declinations within core of 0°. Large declination shifts are apparent at 21 and 66 mcd (Figure 5). These levels are at the tops of cores 1089B-3H (20.74–28.00 mcd) and 1089C-8H (66.30–72.40 mcd), respectively. Because these declination changes are not observed in overlapping cores, these anomalies are attributed to sediment twisting during the APC coring process.

[16] At Site 1089, we observe two intervals of positive inclination and several intervals of shallow inclination with high-amplitude declination swings, associated with poorly defined component directions denoted by high MAD values (Figure 5). The younger of the two intervals of positive inclination occurs at ~29.6 mcd or ~189.5 ka (Figures 10a and 11a). This interval of anomalous direction is almost coeval with the Iceland Basin event, identified at ODP Sites 983 and 984 where it is dated by oxygen isotope stratigraphy to occur between 186 and 189 ka [*Channell et al.*, 1997; *Channell*, 1999]. MAD values calculated for 25–50 mT peak field demagnet-

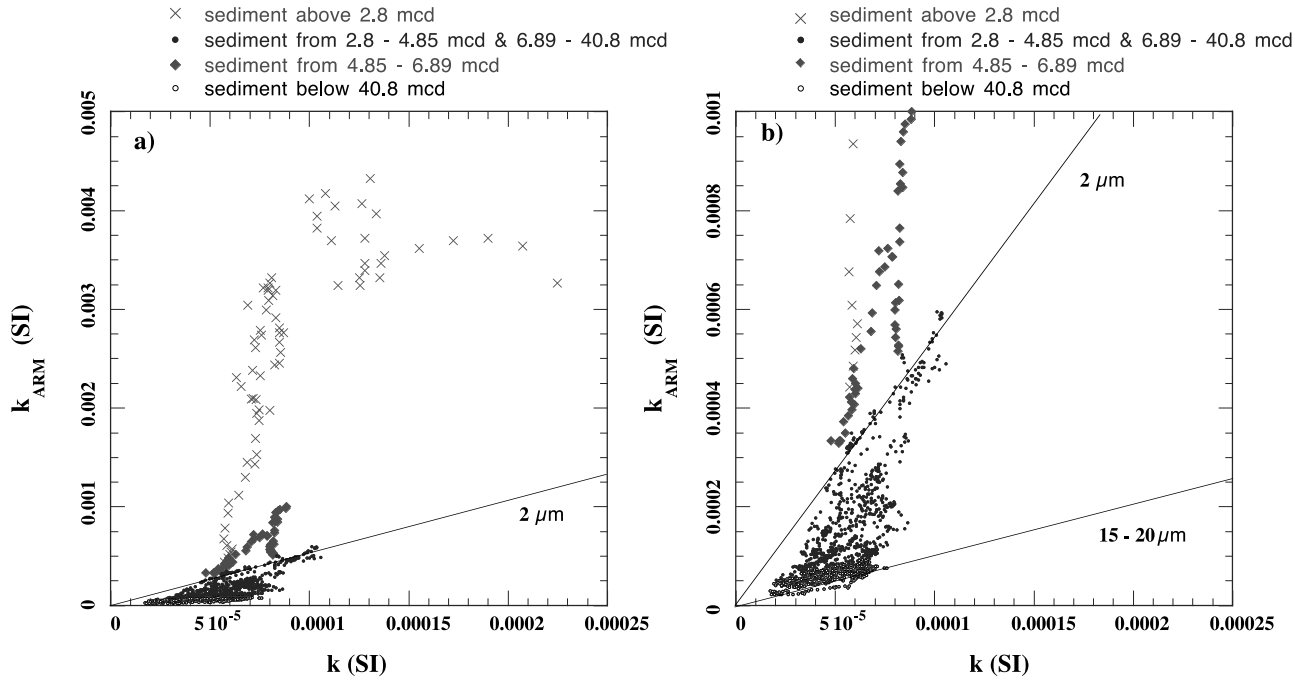

Figure 9. Anhysteretic susceptibility (k_{ARM}) plotted against volume susceptibility (k) at two scales. (a) Complete Site 1089 record. Different symbols correspond to different size populations occurring over distinct stratigraphic intervals as noted in legend. (b) Blowup of the k_{ARM} scale that removes the ultrafine magnetic particles that occur above 2.8 mcd. Changes in slope indicate changes in magnetic grain size [*Banerjee et al.*, 1981]. Lines indicate magnetite grain sizes of ~2 and ~15–20 μm [*King et al.*, 1983]. See color version of this figure in the HTML.

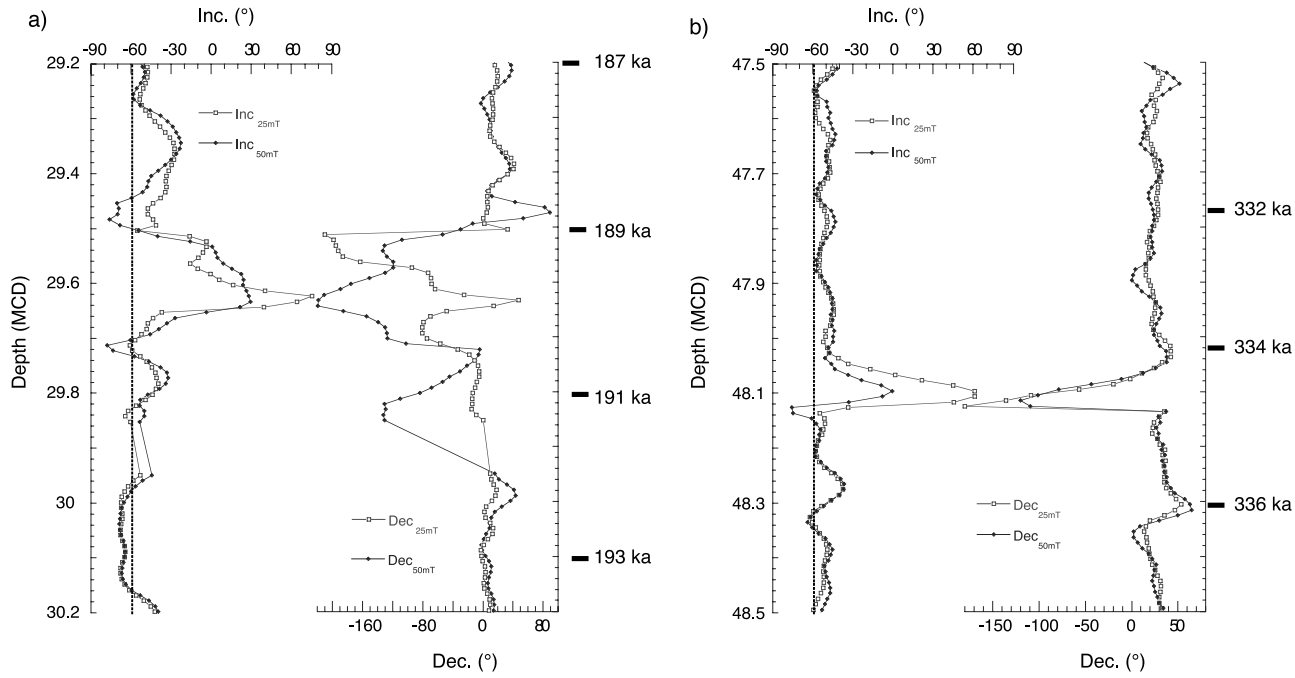

Figure 10. (a) Inclination and declination at 25 and 50 mT peak field AF demagnetization steps for the 29.2–30.2 mcd (~187–194 ka) interval from Site 1089. (b) Inclination and declination at 25 and 50 mT peak field AF demagnetization steps for the 47.5–48.5 mcd (~330–337.5 ka) interval. Vertical line indicates expected inclination (60°) for site latitude. See color version of this figure in the HTML.

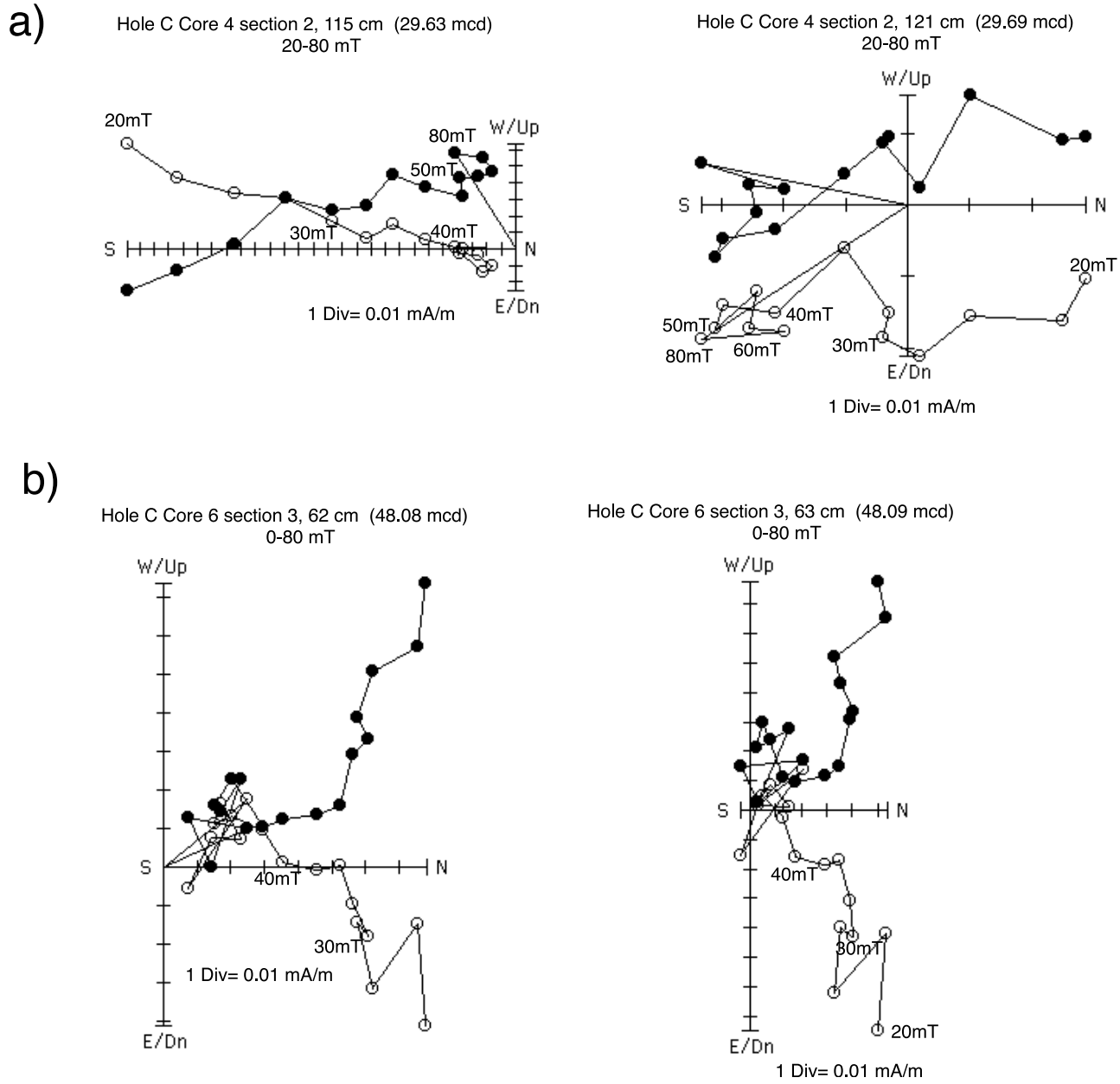

Figure 11. (a) Orthogonal projection of alternating field demagnetization data from u channel measurements at 29.63 and 29.69 mcd recording the magnetic excursion correlative to the Iceland Basin event. Open and solid symbols indicate projection of vector endpoints on the vertical and horizontal planes, respectively. Declinations have been corrected for a core mean of 0° as described in text. The magnetization intensity associated with one division on the axes of each plot is indicated. Peak alternating fields are indicated in mT. (b) Orthogonal projection of alternating field demagnetization data from u channel measurements at 48.08–48.09 mcd interval recording the magnetic excursion at ~334.5 ka.

ization are high (>20°) (Figure 5) consistent with poorly defined magnetization components and overprinting by the postexcursional field (Figure 11a). Figure 10a shows the inclination and declination values at peak AF fields of 25 and 50 mT and illustrates the complex behavior within this interval. The smoothing of the high-coercivity inclination and what appears to be downward displaced declination could reflect a delay in remanence acquisition of the high-coercivity (authigenic pyrrhotite) component.

[17] The older interval of positive inclinations found at ~48.1 mcd (Figures 5, 10b, and 11b) has an estimated age of 334.5 ka. This age is consistent with one of the excursions documented from ODP Leg 172 (9-b) [*Lund et al.*, 1998, 2001]. Orthogonal projections of demagnetization data that define the excursional directions are consistent with overprinting by the postexcursional field (Figure 11b).

6. Normalized Remanent Magnetization (Relative Paleointensity Estimates)

[18] Deriving proxy records of relative geomagnetic paleointensity from sediments involves normalizing the NRM by

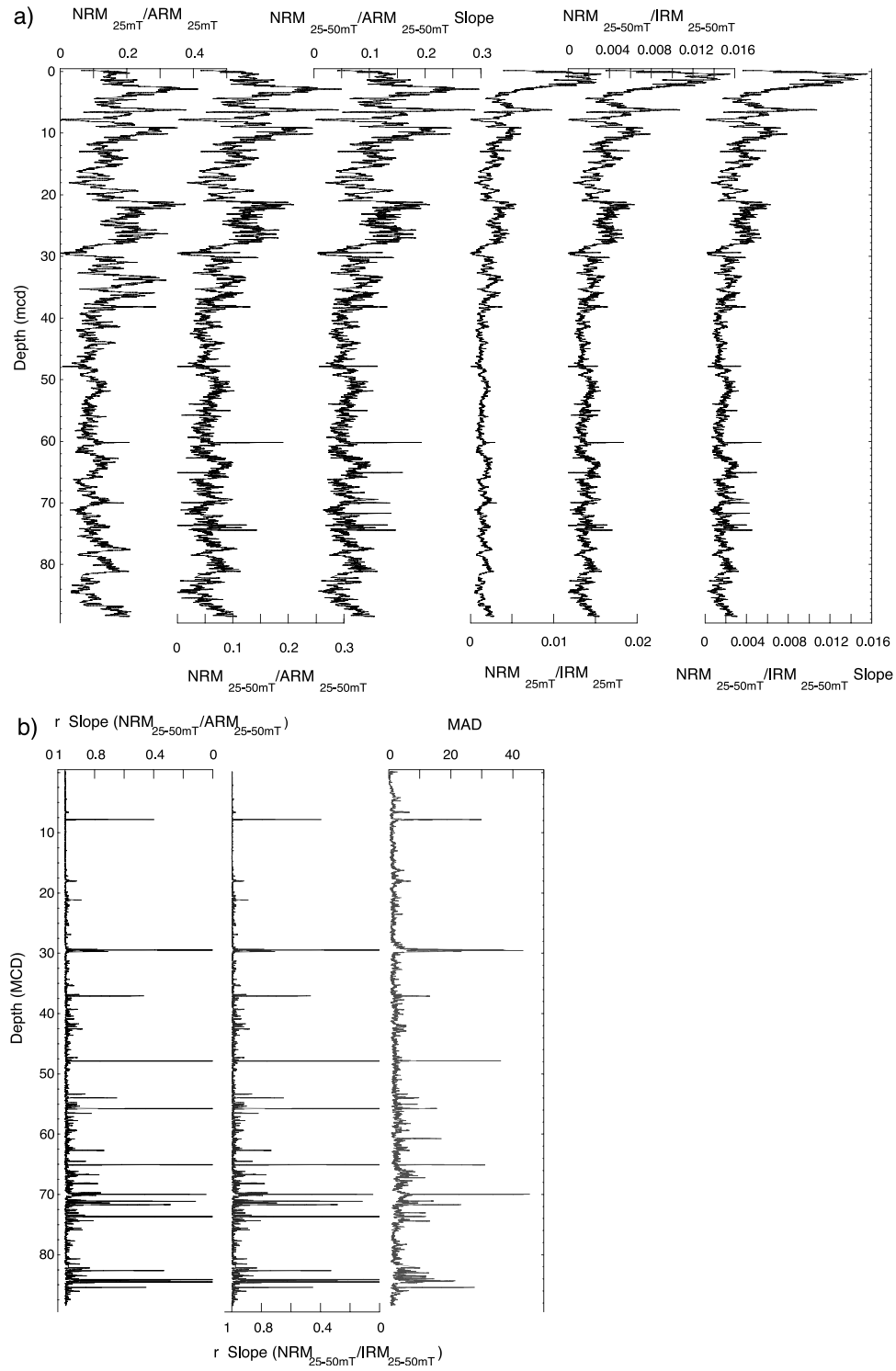

Figure 12. (a) Down-core comparison of different NRM intensity normalization techniques (paleointensity proxies): from left to right, NRM_{25mT}/ARM_{25mT}, Slope of $(NRM_{25mT}\text{-}NRM_{50mT})/(ARM_{25mT}\text{-}ARM_{50mT})$, subtracted vector $(NRM_{25mT}\text{-}NRM_{50mT})/(ARM_{25mT}\text{-}ARM_{50mT})$, NRM_{25mT}/IRM_{25mT}, slope of $(NRM_{25mT}\text{-}NRM_{50mT})/(IRM_{25mT}\text{-}IRM_{50mT})$, subtracted vector $(NRM_{25mT}\text{-}NRM_{50mT})/(IRM_{25mT}\text{-}IRM_{50mT})$. (b) Error estimates, from left to right linear correlation coefficient (r) for slope of $(NRM_{25mT}\text{-}NRM_{50mT})/(ARM_{25mT}\text{-}ARM_{50mT})$, linear correlation coefficient (r) for slope of $(NRM_{25mT}\text{-}NRM_{50mT})/(IRM_{25mT}\text{-}IRM_{50mT})$, MAD values as in Figure 5.

a magnetic parameter that compensates for change in the concentration of NRM-carrying grains. The use of anhysteretic remanent magnetization (ARM) as a normalizer has been placed on a firm theoretical and empirical basis by *King et al.* [1983]. According to these authors, the NRM/ARM ratio can be used as a paleointensity proxy if the NRM is a detrital remanent magnetization (DRM), and is carried by magnetite in the 1–15 μm (SD/PSD) grain-size range. The restricted grain-size range is due to the grain size dependence of both ARM acquisition and NRM retention. Submicron

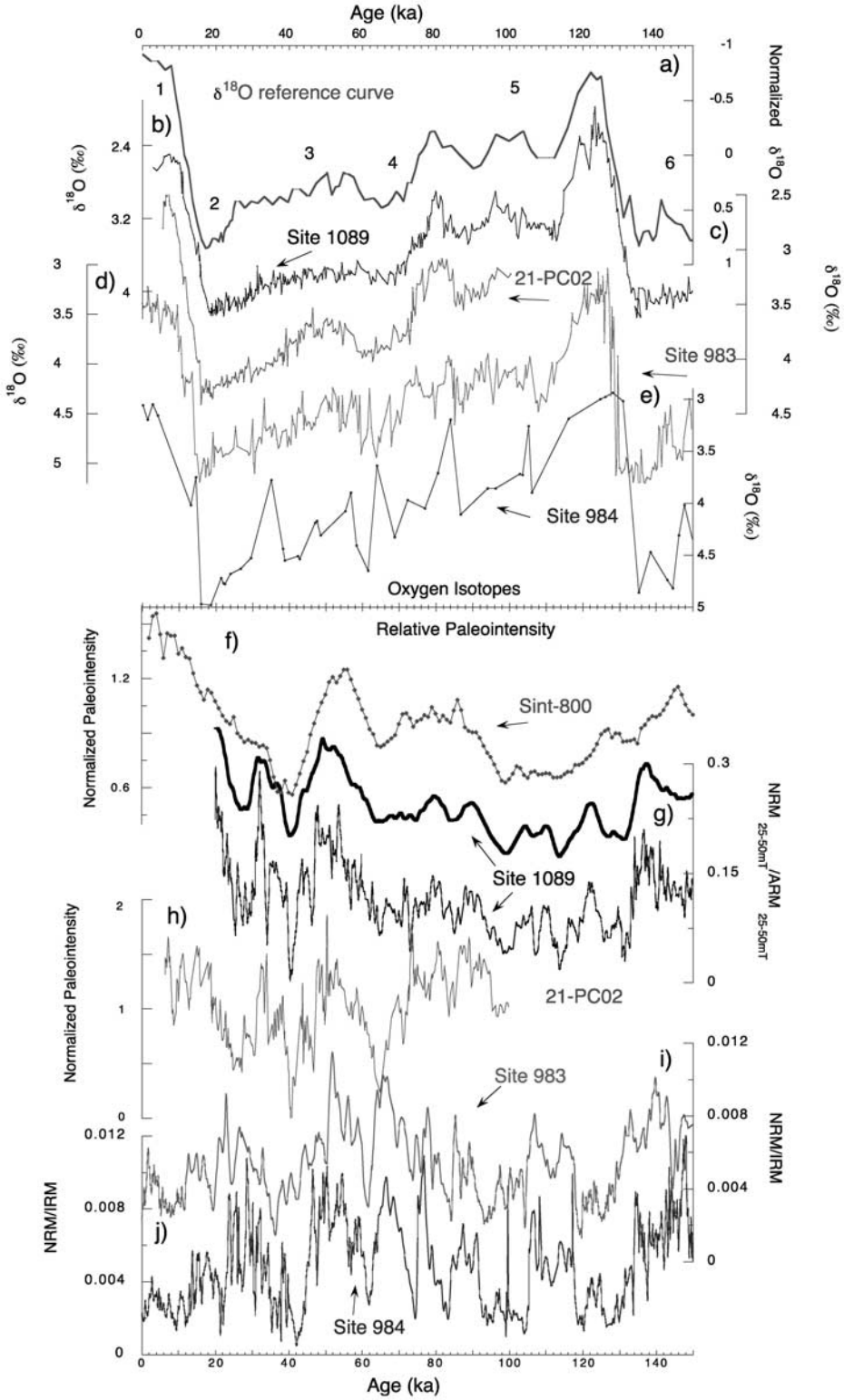

grains and coarse MD magnetite grains are efficient carriers of ARM but relatively inefficient carriers of stable DRM. Concentrations of magnetite should not vary down core by more than a factor of 20–30, because of the effect of particle interactions on the efficiency of ARM acquisition. Demagnetization of both NRM and ARM in the NRM/ARM ratio serves to restrict the grain-size range contributing to both remanences. Besides ARM, isothermal remanent magnetization (IRM) and low field susceptibility (k) have been used as normalizers to derive paleointensity proxies from sediments, although the theoretical basis for the use of IRM or susceptibility (k) has not been adequately documented.

[19] Site 1089 sediments have undergone reductive diagenesis, which has resulted in the growth of iron sulfide (pyrite and pyrrhotite) and down-core dissolution of magnetite. For this reason, the magnetic mineralogy and grain size at Site 1089 are not ideal for paleointensity determinations. Magnetic homogeneity has been considered a critical factor for deriving reliable relative paleointensity estimates [*King et al.*, 1983; *Tauxe*, 1993]. At Site 1089, the sediments are not magnetically homogenous. Below the large remanence drop that occurs within the topmost few meters, ARM intensity values change by almost a factor of 30 and $IRM_{0.3T}$ by slightly more than an order of magnitude (Figure 8). Both these concentration changes are outside the limits advocated by *Tauxe* [1993] for paleointensity determinations from sediments.

[20] To minimize the influence of the high-coercivity (pyrrhotite) contribution we use the subtracted vector normalization method. This reduces the influence of the high-coercivity component by subtracting out that part of the vector. In Figure 13, the subtracted vector normalized remanence (NRM/ARM and NRM/IRM) is derived by subtracting the remanence measured after 50 mT peak demagnetization from that measured after 25 mT peak demagnetization. This normalization is compared with normalized remanence derived from the slopes of the NRM versus ARM (and versus IRM) plots in the chosen coercivity window (25–50 mT), and direct normalization by ARM and IRM at a specific demagnetization level (25 mT). Except for the upper 2.8 mcd, which we suspect contains biogenic magnetite, comparable results are obtained for each normalization technique and each normalizer (ARM and IRM) (Figure 12). The normalized remanence records, however, show a down-core decrease in mean value and amplitude that parallels the diagenetic changes in the magnetic assemblage (Figure 12). To determine whether these sediments are recording past paleointensity changes, we have subdivided the normalized remanence record into 4 intervals, of ~150 kyr, that are relatively homogeneous when compared with the entire magnetic record. The normalized remanence records at Site 1089 can be assessed by comparison with other high-resolution normalized remanence records of the same age, such as those from the ODP Leg 177 site survey cores [*Channell et al.*, 2000], and those from the Iceland Basin [*Channell*, 1999].

6.1. The 0–150 ka Interval

[21] The upper interval extends from 20 to 150 ka (3–23.8 mcd), and it is within this interval where most of the reduction diagenesis has occurred. Magnetic concentration variations are greatest in this interval, changing by a factor of 7 and 16 for IRM and ARM, respectively (after AF demagnetization at 30 mT peak field). For most of the last 150 kyr, the general form of the geomagnetic paleointensity record is reasonably well known at both high and low frequencies, particularly for the Atlantic realm [*Channell et al.*, 2000; *Laj et al.*, 2000; *Stoner et al.*, 2000; *Guyodo and Valet*, 1996, 1999]. Figure 13 illustrates oxygen isotope and normalized remanence records for the 0–150 ka interval. The Site 1089 normalized remanence record (NRM_{25-50}/ARM_{25-50}) compares favorably with relative paleointensity records from ODP Sites 983 and 984 in the Iceland Basin [*Channell et al.*, 1997; *Channell*, 1999], piston core TTN057-21-PC02 from the sub-Antarctic South Atlantic [*Channell et al.*, 2000] and the Sint-200 global paleointensity composite [*Guyodo and Valet*, 1996]. To facilitate comparison of the Site 1089 paleointensity record with the lower-resolution Sint-200 paleointensity stack, we have smoothed the Site 1089 normalized remanence record. This was done by extracting every fourth measurement from the original data to compensate for the smoothing inherent in u channel measurements [*Weeks et al.*, 1993]. These measurement values were then interpolated at equal spacing of 200 years, and then smoothed using a 20 point (4 kyr) running mean (Figure 13).

[22] The Site 1089 normalized remanence record is comparable with other globally distributed high-resolution records that cover this time interval [e.g., *Meynadier et al.*, 1992; *Tric et al.*, 1992; *Stoner et al.*, 1998; *Channell*, 1999; *Laj et al.*, 2000]. Because the rock magnetic properties and diagenetic history of sediments from the sub-Antarctic South Atlantic and Iceland Basin are significantly different, the similarity of the normalized remanence records suggest that, for this time interval, geomagnetic paleointensity variations are recorded and preserved within the Site 1089 record. As each record is shown on its originally published chronology, temporal offset of features

Figure 13. (opposite) Benthic oxygen isotope and relative paleointensity records on their own chronologies for 0–150 ka (a) $\delta^{18}O$ reference curve as in Figure 2. Numbers indicate corresponding marine isotopic stage. (b) Sub-Antarctic South Atlantic ODP Site 1089 benthic $\delta^{18}O$ *C. wuellerstorfi* and *C. kullenbergi* [see *Hodell et al.*, 2001; *Mortyn et al.*, 2003]. (c) Sub-Antarctic South Atlantic piston core 21-PC02 benthic $\delta^{18}O$ *Cibicidoides wuellerstorfi* [*NinneMann et al.*, 1999]. (d) North Atlantic ODP Site 983 benthic $\delta^{18}O$ from *C. wuellerstorfi* [*Channell et al.*, 1997]. (e) North Atlantic ODP Site 984 benthic $\delta^{18}O$ from *C. wuellerstorfi* [*Channell et al.*, 1998]. (f) Sint-200 paleointensity record [*Guyodo and Valet*, 1996]. (g) Site 1089 relative paleointensity estimated from the subtracted vector $(NRM_{25mT}\text{-}NRM_{50mT})/(ARM_{25mT}\text{-}ARM_{50mT})$ normalization method. Displayed as a 4000 year running mean, above and below the unsmoothed record. The chronology for Site 1089 defined in Figure 2. (h) 21-PC02 paleointensity record [*Channell et al.*, 2000]. (i) Site 983 paleointensity record [*Channell et al.*, 1997; *Channell*, 1999]. (j). Site 984 paleointensity record [*Channell et al.*, 1998; *Channell*, 1999]. See color version of this figure in the HTML.

may be due to chronological imprecision. For example, in Figure 13, the easily recognizable paleointensity low, associated with the Laschamp geomagnetic excursion, varies in age from ~32 ka at Site 983 to ~40 ka at Site 1089. An age of ~40 ka has been estimated for the Laschamp event in North Atlantic cores placed on a GISP2 (Greenland) ice core chronology [*Laj et al.*, 2000]. Although temporal discrepancies are readily apparent when comparing paleointensity records, most of the oxygen isotope records, on which the age models are generally based, suggest that the records are reasonably well synchronized (Figure 13).

6.2. The 150–300 ka Interval

[23] For the 150–300 ka interval (23–43 mcd), IRM and ARM (magnetic concentration parameters) vary by a factor of 4 and 5, respectively, after AF demagnetization at peak fields of 30 mT. The Site 1089 normalized remanence record (NRM_{25-50}/ARM_{25-50}) in the 150–300 ka interval (Figure 14) shows no obvious down-core trend. The Iceland Basin paleointensity records (ODP Sites 983 and 984), the Sint-800 global paleointensity composite [*Guyodo and Valet*, 1999], and the Site 1089 normalized remanence record show a paleointensity low at ~186–190 ka associated with a geomagnetic excursion known as the Iceland Basin event [*Channell et al.*, 1997; *Channell*, 1999]. Prior to 190 ka, mismatches between the normalized remanence features are observed (Figure 14) which could reflect chronological error. By optimizing the correlation of the Site 1089 and Site 983 paleointensity records, the correlation coefficient of the two paleointensity records can be improved (from r = 0.363 to r = 0.706) without violating the isotope stratigraphy.

6.3. The 300–450 ka Interval

[24] For the 300–450 ka interval (43–69.5 mcd), concentration-related magnetic parameters vary by a factor of ~5 for both IRM and ARM after peak field AF demagnetization at 30 mT (Figure 8). Grain-size changes as indicated by the ratio k_{ARM}/k are negligible in this interval (Figure 9). Comparison of the Site 1089 normalized remanence record with those from ODP Sites 983 and 984 show many similar features (Figure 15) suggesting that these changes are reflecting variations in geomagnetic paleointensity. When comparing the smoothed Site 1089 record to the Sint-800 composite stack [*Guyodo and Valet*, 1999] clear temporally discrepancies are observed.

6.4. The 450–580 ka Interval

[25] For the 450–580 ka interval (69.5–89 mcd), magnetic concentration parameters vary by a factor of ~3, as measured by both IRM and ARM (Figure 8). Comparison of the Site 1089 normalized remanence record with those from Sites 983 and 984 show poor correlation (Figure 16) relative to the younger intervals. The smoothed Site 1089 record, though temporally offset, is quite similar to the Sint-800 record.

7. Discussion and Conclusions

[26] High deposition rate sediments at ODP Site 1089 in sub-Antarctic South Atlantic give normalized remanence records similar to those observed in high deposition rate sediments from the North Atlantic (Sites 983 and 984). Magnetite is the principal remanence carrier throughout the section, although part of the initial magnetite content is lost due to reductive diagenesis. The reduction of magnetite to iron sulfide (pyrite/pyrrhotite) occurs within the uppermost few meters of the sediment column. Removal of an inferred biogenic magnetite component is indicated by the abrupt drop in magnetic remanence intensities and coarser magnetic assemblage below ~2.8 mcd. Below this depth, the down-core reduction in magnetization intensities follows the pore water sulfate concentration profile that reaches zero at ~50 mcd [*Shipboard Scientific Party*, 1999]. Below 50 mcd, magnetite dissolution is probably negligible as the process is probably sulfate limited in these sediments [see *Canfield and Berner*, 1987]. The low-coercivity magnetization component carries a clear polarity stratigraphy down to the base of the Olduvai Subchronozone at 250 mcd [*Channell and Stoner*, 2002] indicating that the dissolution process has affected only a portion of the NRM-carrying magnetite grains. These grains record two short intervals of excursional directions within the Brunhes Chronozone (Figures 5, 10, and 11). Although the excursional directions are heavily overprinted by the postexcursional field, the younger of these occurs at 189–190 ka and is approximately coeval with the Iceland Basin event found at ODP Sites 983 and 984 [*Channell*, 1999], suggesting that this event may be manifest globally. The older excursional interval, also heavily overprinted, occurs during MIS 9 at ~335 ka and appears to be correlative to one of the excursions documented from ODP Leg 172 [*Lund et al.*, 1998, 2001]. Other excursions, such as the now well-established Laschamp event [e.g., *Laj et al.*, 2000] have been recorded in nearby piston cores [*Channell et al.*, 2000]. At Site 1089, the Laschamp event appears to be manifested (at 7.8 mcd) as anomalously high-amplitude secular variation and high MAD values (Figure 5), indicating poorly defined excursional directions, and low normalized remanence values (Figures 12 and 13).

[27] These sediments are not ideally suited for derivation of relative paleointensity proxies because of down-core dissolution of magnetite and the apparent presence of pyrrhotite. The magnetic properties are, however, relatively homogeneous over short stratigraphic intervals and the normalized remanence records within these intervals are comparable with relative paleointensity records from the Northern Hemisphere (Figures 13–16). This suggests that by removing the down-core trend in the normalized remanence record (see Figure 12), a useful and continuous paleointensity proxy record may be derived. In Figure 17, the Site 1089 normalized remanence record was detrended using a sixth-order polynomial derived from the smoothed data set. To account for the reduction in amplitude in the lower part of the record, we rescaled the record to a common standard deviation. The oxygen isotope records and the detrended normalized remanence record from ODP Site 1089 were then optimally correlated with the oxygen isotope records and similarly smoothed paleointensity data from ODP Site 983, using Analyseries software [*Paillard et al.*, 1996]. The Site 983 chronology was thereby adjusted to that of Site 1089, with a resulting improvement in correlation of both the oxygen isotope (from r = 0.812 to 0.89) and paleointensity proxies (from r = 0.381 to 0.575). After this correlation exercise, the Site 1089 and Site 983 oxygen

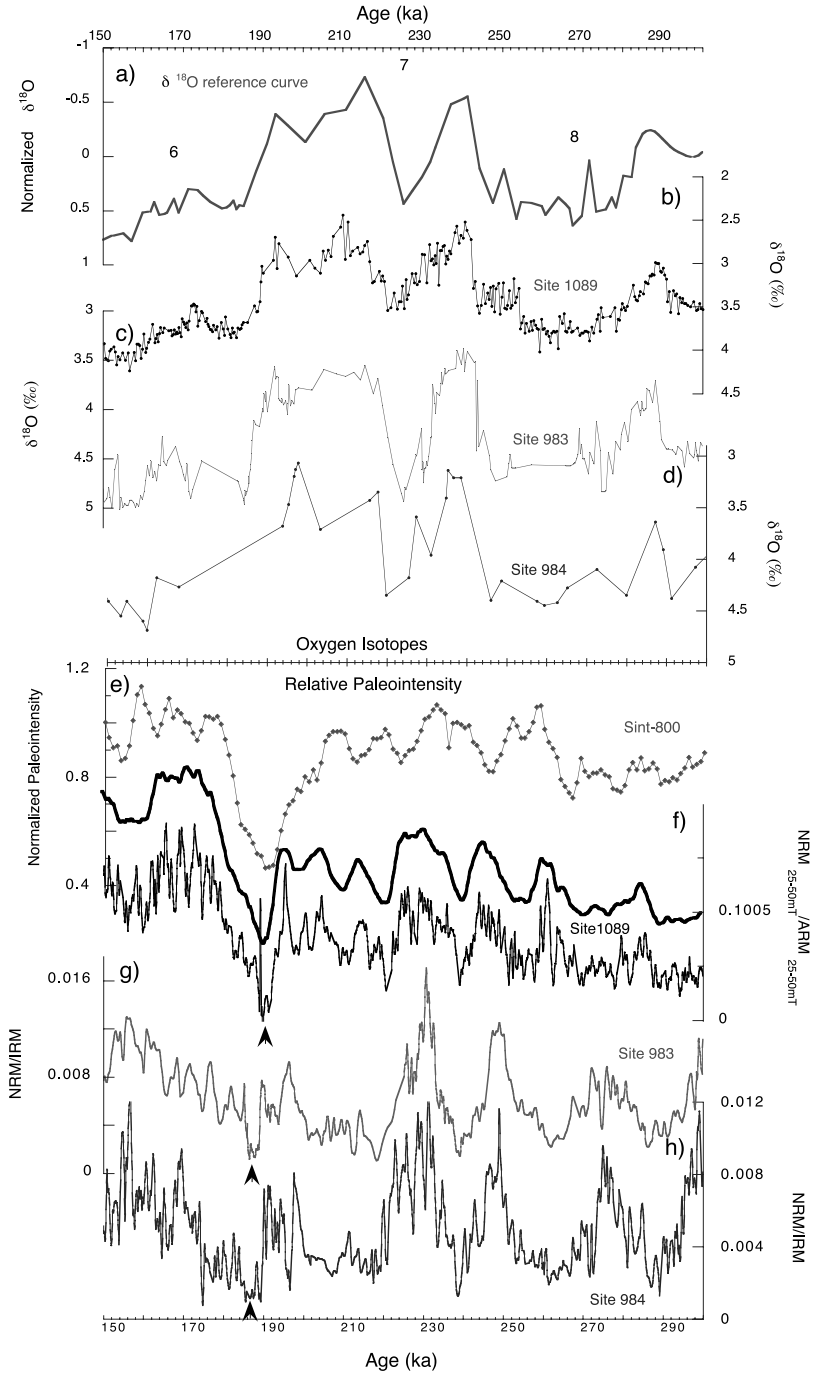

Figure 14. Benthic oxygen isotope and paleointensity records on their individual chronologies for 150–300 ka. (a) The $\delta^{18}O$ reference curve as in Figure 2. Numbers indicate corresponding marine isotopic stage. (b) Sub-Antarctic South Atlantic ODP Site 1089 benthic $\delta^{18}O$ *C. wuellerstorfi* and *C. kullenbergi* and from 190 to 220 ka the planktic $\delta^{18}O$ *G. bulloides* spliced into the benthic record [see *Hodell et al.*, 2001; *Mortyn et al.*, 2003] on the chronology derived in Figure 2. (c) North Atlantic ODP Site 983 benthic $\delta^{18}O$ from *C. wuellerstorfi* [*Channell et al.*, 1997]. (d) North Atlantic ODP Site 984 benthic $\delta^{18}O$ from *C. wuellerstorfi* [*Channell et al.*, 1998]. (e) Sint-800 paleointensity record [*Guyodo and Valet*, 1999]. (f) Site 1089 relative paleointensity estimated from the subtracted vector (NRM_{25mT}-NRM_{50mT})/(ARM_{25mT}-ARM_{50mT}) normalization method. Displayed as a 4000 year running mean, above and below the unsmoothed record. The chronology for Site 1089 defined in Figure 2. (g) Site 983 paleointensity record [*Channell et al.*, 1997; *Channell*, 1999]. (h) Site 984 paleointensity record [*Channell et al.*, 1998; *Channell*, 1999]. Arrows indicate the stratigraphic position of the excursional directions (Iceland Basin Event) in each period (Figures 10a and 11a). See color version of this figure in the HTML.

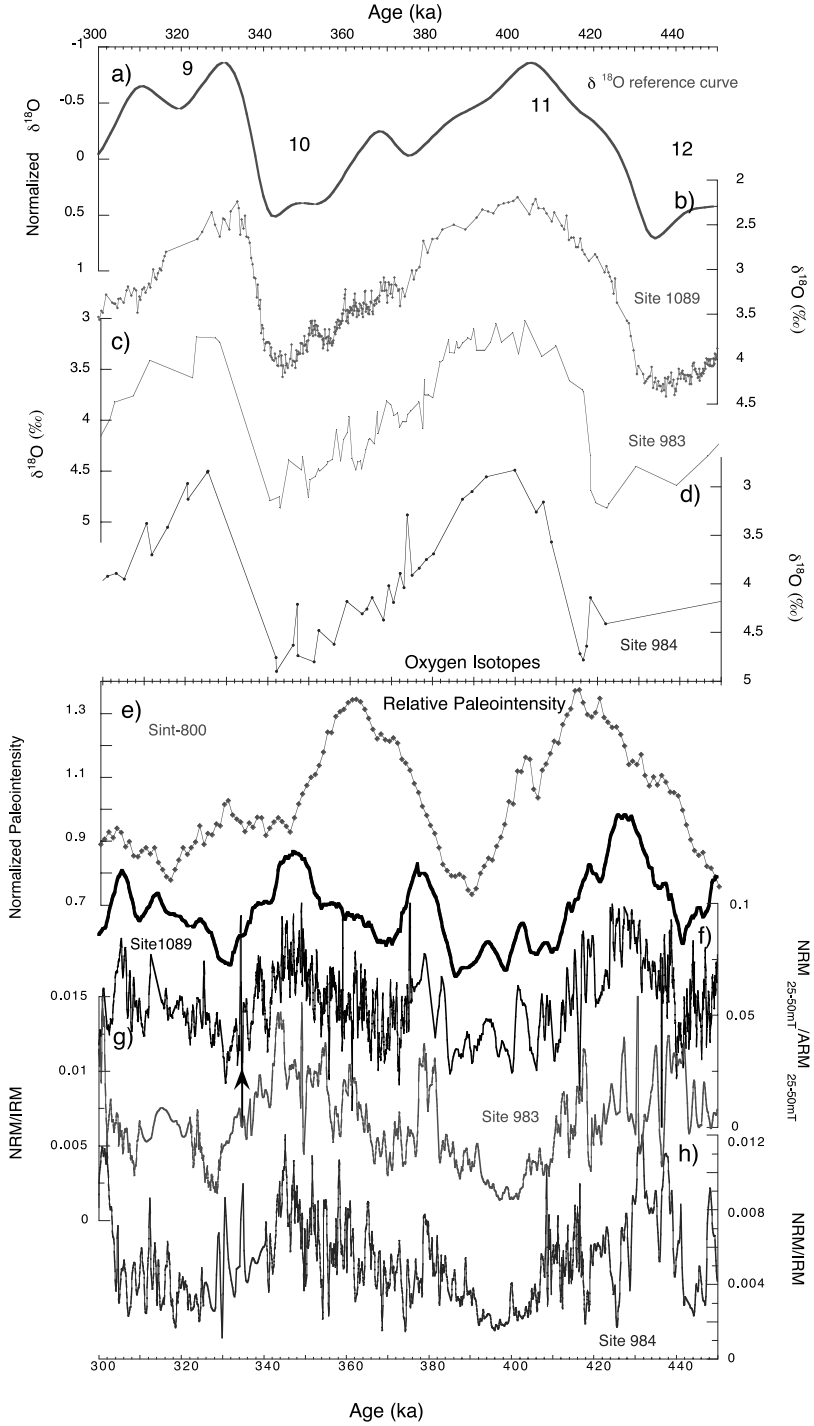

Figure 15. Benthic oxygen isotope and paleointensity records on their individual chronologies for 300–450 ka. (a) The $\delta^{18}O$ reference curve as in Figure 2. Numbers indicate corresponding marine isotopic stage. (b) Sub-Antarctic South Atlantic ODP Site 1089 benthic $\delta^{18}O$ *C. wuellerstorfi* and *C. kullenbergi* and planktic $\delta^{18}O$ *G. bulloides* [see *Hodell et al.*, 2001; *Mortyn et al.*, 2003] on the chronology derived in Figure 2. (c) North Atlantic ODP Site 983 benthic $\delta^{18}O$ from *C. wuellerstorfi* [*Channell et al.*, 1998]. (d) North Atlantic ODP Site 984 benthic $\delta^{18}O$ from *C. wuellerstorfi* [*Channell et al.*, 1998]. (e) Sint-800 paleointensity record [*Guyodo and Valet*, 1999]. (f) Site 1089 relative paleointensity estimated from the subtracted vector $(NRM_{25mT}\text{-}NRM_{50mT})/(ARM_{25mT}\text{-}ARM_{50mT})$ normalization method. Displayed as a 4000 year running mean, above and below the unsmoothed record. The chronology for Site 1089 defined in Figure 2. (g) Site 983 paleointensity [*Channell et al.*, 1997; *Channell*, 1999] (h) Site 984 paleointensity record [*Channell et al.*, 1998; *Channell*, 1999]. Arrow indicates the stratigraphic position of the excursional directions in Site 1089 (Figures 10b and 11b). See color version of this figure in the HTML.

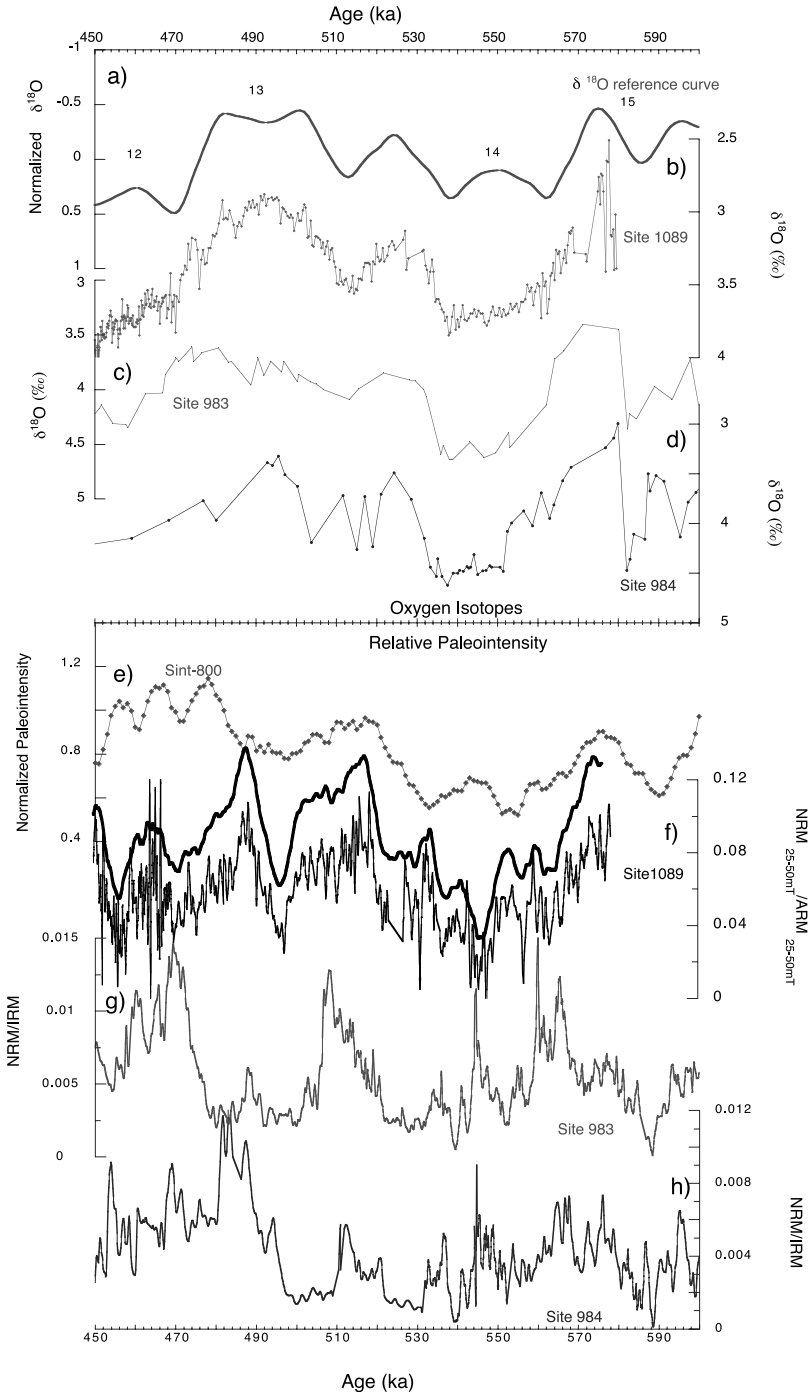

Figure 16. Benthic oxygen isotope and relative paleointensity records on their individual chronologies for 450–600 ka. (a) The $\delta^{18}O$ reference curve as in Figure 2. Numbers indicate corresponding marine isotopic stage. (b) Sub-Antarctic South Atlantic ODP Site 1089 benthic $\delta^{18}O$ *C. wuellerstorfi* and *C. kullenbergi* and planktic $\delta^{18}O$ *G. bulloides* [see *Hodell et al.*, 2001; *Mortyn et al.*, 2003] on the chronology derived in Figure 2. (c) North Atlantic ODP Site 983 benthic $\delta^{18}O$ from *C. wuellerstorfi* [*Channell et al.*, 1998]. (d) North Atlantic ODP Site 984 benthic $\delta^{18}O$ from *C. wuellerstorfi* [*Channell et al.*, 1998]. (e) Sint-800 paleointensity record [*Guyodo and Valet*, 1999]. (f) Site 1089 relative paleointensity estimated from the subtracted vector $(NRM_{25mT}\text{-}NRM_{50mT})/(ARM_{25mT}\text{-}ARM_{50mT})$ normalization method. Displayed as a 4000 year running mean, above and below the unsmoothed record. The chronology for Site 1089 defined in Figure 2. (g) Site 983 paleointensity [*Channell et al.*, 1997; *Channell*, 1999]. (h) Site 984 paleointensity record [*Channell et al.*, 1998; *Channell*, 1999]. See color version of this figure in the HTML.

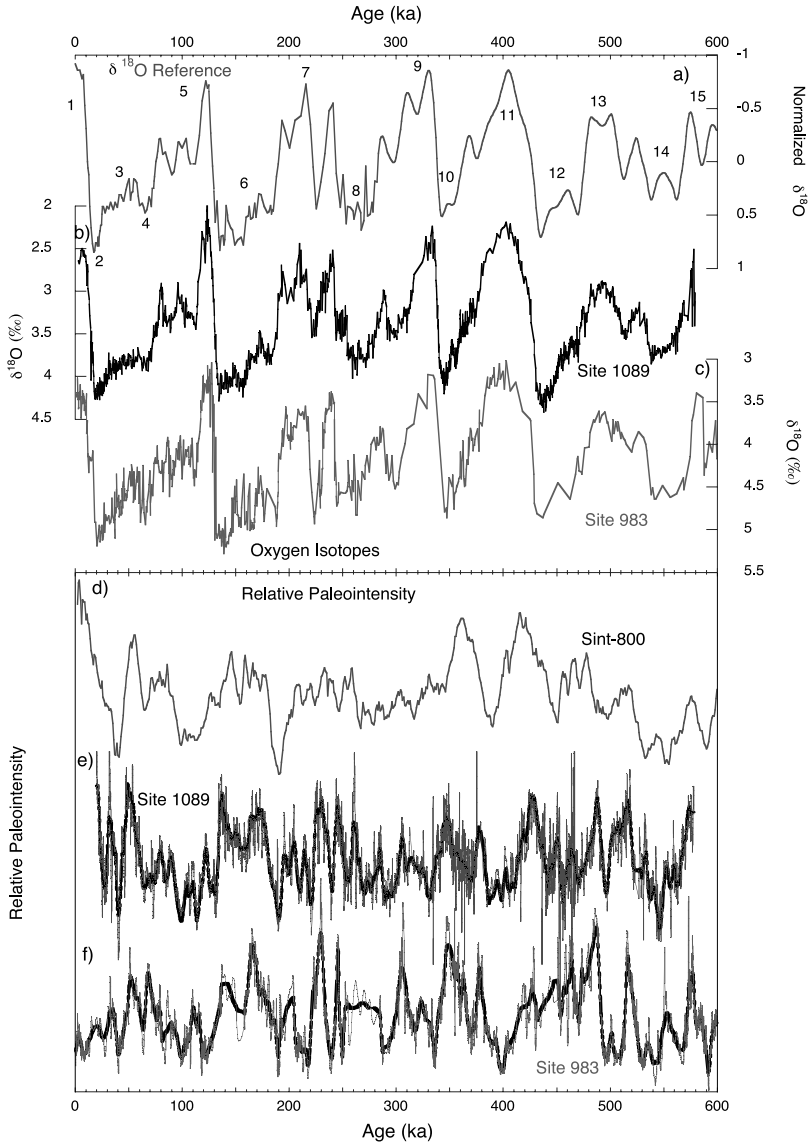

Figure 17. Benthic oxygen isotope and relative paleointensity records on a common chronology for the last 600 ka. (a) The $\delta^{18}O$ reference curve as in Figure 2. Numbers indicate corresponding marine isotopic stage. (b) Sub-Antarctic South Atlantic ODP Site 1089 benthic $\delta^{18}O$ *C. wuellerstorfi* and *C. kullenbergi* and planktic $\delta^{18}O$ *G. bulloides* [see [*Hodell et al.*, 2001; *Mortyn et al.*, 2003] on the chronology derived in Figure 2. Planktic isotope data are spliced into benthic isotope gap from 190 to 220 ka to provide a continuous record. (c) North Atlantic ODP Site 983 benthic $\delta^{18}O$ from *C. wuellerstorfi* [*Channell et al.*, 1998] placed on a new chronology (see text). (d) Sint-800 paleointensity record [*Guyodo and Valet*, 1999]. (e) Site 1089 relative paleointensity estimated derived from the subtracted vector (NRM_{25mT}-NRM_{50mT})/(ARM_{25mT}-ARM_{50mT}) normalization method. The down-core trend has been removed and the record rescaled to a common standard deviation. Curve is smoothed by a 4 kyr running mean. (f) Site 983 paleointensity [*Channell et al.*, 1997; *Channell*, 1999] placed on a new chronology (see text). Curve is smoothed by a 4 kyr running mean. See color version of this figure in the HTML.

isotope records are well correlated to the SPECMAP reference curve (r = 0.904 and 0.818 respectively). The Site 1089 and Site 983 paleointensity records do not, however, correlate well with the Sint-800 paleointensity stack (r = 0.428 and 0.289, respectively).

[28] The correlation of features in the normalized remanence records between the South Atlantic (Site 1089) and Iceland Basin (Sites 983 and 984) cannot be attributed to the influence of climate/lithology due to the predominantly out-of-phase character of millennial-scale climate variability at the two locations [*Charles et al.*, 1996]. On longer timescales, ODP Site 1089 has a "Pacific-type" carbonate stratigraphy [*Hodell et al.*, 2001] with high carbonate content during glacials, and low carbonate during interglacials, while ODP Sites 983 and 984 have an "Atlantic-type" carbonate stratigraphy characterized by the opposite pattern. Lithologic variations at Sites 1089 and 983 would therefore be expected to be out of phase.

[29] The similarity of paleointensity proxy records between the North Atlantic and South Atlantic (Figure 17) suggests that the input geomagnetic signal is essentially global, but that the output is perturbed by the vagaries of stochastic sedimentation, the NRM recording process and postdepositional diagenetic transformations. This study illustrates the potential of combining oxygen isotope data with geomagnetic paleointensity proxies as a means of global stratigraphic correlation and demonstrates that paleointensity, through its role as a correlation tool, will provide powerful new constraints on the processes that drive Quaternary climate change.

[30] **Acknowledgments.** We thank the Captain and the crew of the R/V *Joides Resolution* and the ODP staff at the Bremen core repository. Reviews by S. Brackfeld, M. Tivey, and an anonymous reviewer improved the manuscript. G. Acton, and N. Shackleton provided comments on an early version of this manuscript. This work was financially supported by the U.S. Science Support Program (USSSP), administered by Texas A&M University, and by the U.S. National Science Foundation (OCE-9711424 and OCE-9911698).

References

Banerjee, S. K., J. King, and J. Marvin, A rapid method for magnetic granulometry with applications to environmental studies, *Geophys. Res. Lett.*, *8*, 333–336, 1981.

Canfield, D. E., and R. A. Berner, Dissolution and pyritization of magnetite in anoxic marine sediments, *Geochim. Cosmochim. Acta*, *51*, 645–659, 1987.

Channell, J. E. T., Geomagnetic paleointensity and directional secular variation at Ocean Drilling Program (ODP) Site 984(Bjorn Drift) since 500 ka: Comparisons with ODP Site 983(Gardar Drift), *J. Geophys. Res.*, *104*, 22,937–22,952, 1999.

Channell, J. E. T., and C. McCabe, Comparison of magnetic hysteresis parameters of unremagnetized and remagnetized limestones, *J. Geophys. Res.*, *99*, 4613–4623, 1994.

Channell, J. E. T., and J. S. Stoner, Plio-Pleistocene magnetic polarity stratigraphies and diagenetic magnetite dissolution at ODP Leg 177 Sites (1089, 1091, 1093 and 1094), *Mar. Micropaleontol.*, *45*, 269–290, 2002.

Channell, J. E. T., D. A. Hodell, and B. Lehman, Relative geomagnetic paleointensity and d^{18}O at ODP Site 983(Gardar Drift, North Atlantic) since 350 ka, *Earth Planet. Sci. Lett.*, *153*, 103–118, 1997.

Channell, J. E. T., D. A. Hodell, J. McManus, and B. Lehman, Orbital modulation of geomagnetic paleointensity, *Nature*, *394*, 464–468, 1998.

Channell, J. E. T., J. S. Stoner, D. A. Hodell, and C. Charles, Geomagnetic paleointensity from late Brunhes-age piston cores from the sub-Antarctic South Atlantic, *Earth Planet. Sci. Lett.*, *175*, 145–160, 2000.

Charles, C. D., J. Lynch-Stieglitz, U. S. Ninnemann, and R. G. Fairbanks, Climate connections between the hemispheres revealed by deep sea sediment core/ice core correlations, *Earth Planet. Sci. Lett.*, *142*, 19–27, 1996.

Day, R., M. Fuller, and V. A. Schmidt, Hysteresis properties of titanomagnetites: Grain-size and compositional dependence, *Phys. Earth Planet. Inter.*, *13*, 260–267, 1977.

Guyodo, Y., and J. P. Valet, Relative variations in geomagnetic intensity from sedimentary records—The past 200,000 years, *Earth Planet. Sci. Lett.*, *143*, 23–46, 1996.

Guyodo, Y., and J. P. Valet, Global changes in intensity of the Earth's magnetic field during the past 800 kyr, *Nature*, *399*, 249–252, 1999.

Hodell, D. A., C. D. Charles, and F. J. Sierro, Late Pleistocene evolution of the ocean's carbonate system, *Earth Planet. Sci. Lett.*, *192*, 109–124, 2001.

Hodell, D. A., C. D. Charles, J. H. Curtis, P. G. Mortyn, U. S. Ninnemann, and K. A. Venz, Data report: Oxygen isotope stratigraphy of Leg 177 Sites 1088, 1089, 1090, 1093, and 1094, *Proc. Ocean Drill. Program Sci. Results* [online], 177, 2003. (Available at http://www-odp.tamu.edu/publications/177_SR/chap_09/chap_09.htm)

Imbrie, J., J. D. Hays, D. G. Martinson, A. McIntyre, A. Mix, J. J. Morley, N. G. Pisias, W. L. Prell, and N. J. Shackleton, The orbital theory of Pleistocene climate: Support from a revised chronology of the marine d^{18}O record, in *Milankovitch and Climate*, *Nato ASI Ser.*, *Ser. C*, vol. 126, edited by A. L. Berger et al., pp. 269–305, Kluwer Acad., Norwell, Mass., 1984.

King, J. W., S. K. Banerjee, and J. Marvin, A new rock magnetic approach to selecting sediments for geomagnetic intensity studies: Application to paleointensity for the last 4000 years, *J. Geophys. Res.*, *88*, 5911–5921, 1983.

Kirschvink, J. L., The least squares lines and plane analysis of Paleomagnetic data, *Geophys. J. R. Astron. Soc.*, *62*, 699–718, 1980.

Kuhn, G., and B. Diekman, Late Quaternary variability of oceanic circulation in the southeastern South Atlantic inferred from the terrigenous sediment record of a drift deposit in the southern Cape basin (ODP Site 1089), *Palaeogeogr. Palaeoclimatol. Palaeoecol.*, *182*, 287–303, 2002.

Laj, C., C. Kissel, A. Mazaud, J. E. T. Channell, and J. Beer, North Atlantic Paleointensity Stack since 75 ka (NAPIS-75) and the duration of the Laschamp event, *Philos. Trans. R. Soc., Ser. A*, *358*, 1009–1025, 2000.

Lund, S. P., A comparison of paleomagnetic secular variation records from North America, *J. Geophys. Res.*, *101*, 8007–8024, 1996.

Lund, S. P., G. Acton, B. Clement, M. Hastedt, M. Okada, and T. Williams, Geomagnetic field excursions occurred often during the last million years, *Eos Trans. AGU*, *79*, 178–179, 1998.

Lund, S. P., T. Williams, G. D. Acton, B. Clement, and M. Okada, Brunhes Chron magnetic field excursions recovered from Leg 172 sediments, Proc, *Ocean Drill. Program Sci. Results* [online], *172*, 2001. (Available at http://www-odp.tamu.edu/publications/172_SR/chap_10/chap_10.htm).

Martinson, D. G., N. G. Pisias, J. D. Hays, J. Imbrie, T. C. Moore Jr., and N. J. Shackleton, Age dating and the orbital theory of the Ice Ages: Development of a high-resolution 0 to 300,000-year chronostratigraphy, *Quat. Res.*, *27*, 1–29, 1987.

Meynadier, L., J.-P. Valet, R. Weeks, N. J. Shackleton, and V. L. Hagee, Relative geomagnetic intensity of the field during the last 140 ka, *Earth Planet Sci. Lett.*, *114*, 39–57, 1992.

Mortyn, P. G., C. D. Charles, U. S. Ninnemann, and D. A. Hodell, Deep sea sedimentary analogs for the Vostok ice core, *Geochem. Geophys. Geosyst.*, *4*, doi:10.1029/2002GC000475, in press, 2003.

Ninnemann, U. S., C. D. Charles, and D. A. Hodell, Origin of global millennial scale climate events: Constraints from the Southern Ocean deep sea sedimentary record, in *Mechanisms of Global Climate Change at Millennial Time Scales*, *Geophys. Monogr. Ser.*, vol. 112, edited by P. U. Clark, R. S. Webb, and L. D. Keigwin, pp. 99–112, AGU, Washington, D. C., 1999.

Paillard, D., L. Labeyrie, and P. Yiou, Macintosh program performs time-series analysis, *Eos Trans. AGU*, *77*, 379, 1996.

Shipboard Scientific Party, Site 1089, *Proc. Ocean Drill. Program Initial Rep.* [*CD ROM*], *177*, 1–97, 1999.

Stoner, J. S., J. E. T. Channell, and C. Hillaire-Marcel, A 200 kyr geomagnetic stratigraphy for the Labrador Sea: Indirect correlation of the sediment record to SPECMAP, *Earth Planet. Sci. Lett.*, *159*, 165–181, 1998.

Stoner, J. S., J. E. T. Channell, C. Hillaire-Marcel, and C. Kissel, Geomagnetic paleointensity and environmental record from Labrador Sea Core MD95-2024: Global marine sediment and ice core chronostratigraphy for the last 110 kyr, *Earth Planet. Sci. Lett.*, *183*, 161–177, 2000.

Tauxe, L., Sedimentary records of relative paleointensity of the geomagnetic field: Theory and practice, *Rev. Geophys.*, *31*, 319–354, 1993.

Tauxe, L., J. L. LaBrecque, R. Dodson, and M. Fuller, U-channels—A new technique for paleomagnetic analysis of hydraulic piston cores, *Eos Trans. AGU*, *64*, 219, 1983.

Tric, E., J.-P. Valet, P. Tucholka, M. Paterne, L. Labeyrie, F. Guichard, L. Tauxe, and M. Fontugne, Paleointensity of the geomagnetic field during the last 80,000 years, *J. Geophys. Res.*, *97*, 9337–9351, 1992.

Weeks, R. J., C. Laj, L. Endignoux, M. D. Fuller, A. P. Roberts, R. Manganne, E. Blanchard, and W. Goree, Improvements in long core measurement techniques: applications in palaeomagnetism and palaeoceanography, *Geophys. J. Int.*, *114*, 651–662, 1993.

J. E. T. Channell and D. A. Hodell, Department of Geological Sciences, University of Florida, Gainesville, FL 32611-2120, USA.

C. D. Charles, Scripps Institution of Oceanography, La Jolla, CA 92093-0220, USA.

J. S. Stoner, Institute of Arctic and Alpine Research (INSTAAR), University of Colorado, Boulder, CO 80309-0450, USA. (joseph.stoner@colorado.edu)